Phase Shedding of a Ripple-Free Stacked Interleaved Boost Converter for Fuel Cell-Based Powertrains

Phase Shedding of a Ripple-Free Stacked Interleaved Boost Converter for Fuel Cell-Based Powertrains

Paolo Pilati, *Student Member, IEEE*, Riccardo Mandrioli, *Senior Member, IEEE*, Vincenzo Cirimele, *Senior Member, IEEE*, Damien Guilbert, *Senior Member, IEEE*, Mattia Ricco, *Senior Member, IEEE*

***Abstract*—The necessity of lowering emissions in the transportation sector is driving growing interest in fuel cell electric vehicles. Nonetheless, these vehicles still face several challenges, such as elevated costs and concerns about reliability. This paper explores the impact of the current ripple on PEM fuel cells and presents how a straightforward converter topology can be utilized to address this issue. The study considers a stacked interleaved boost converter. The basis of this converter topology is the interleaved boost, which, with the addition of a dedicated leg, allows for the cancellation of the current ripple for every load condition. Other advantages of this topology are its modularity and the possibility of improving its efficiency at partial loads thanks to phase shedding. The objective of this work is to propose a modulation of this converter topology that maximises efficiency while maintaining ripple-free on the input current. A numerical analysis of the converter's efficiency, simulations of trends in electrical quantities, and experimental validations are performed to investigate the behaviour of the additional leg.**

***Index Terms*—Fuel cell, stacked interleaved boost converter, ripple-free, phase shedding.**

I. Introduction

CURRENTLY, fossil fuels are a primary source for meet the needs of the transport sector. However, their intensive use leads to various negative effects, including air pollution, stratospheric ozone depletion, and global warming, which leads to climate change [1]. Faced with these problems, in recent years the scientific community, industry, and policy makers have turned towards mobility solutions with less environmental impact, promoting the development of Battery Electric Vehicles (BEVs) or Fuel Cell Electric Vehicles (FCEVs) [2]. Fuel cells (FCs), in particular, can be applied in various means of transport, including cars, light commercial vehicles, buses, and trucks, due to their energy-to-weight ratio [3]. This consideration is especially relevant in large-scale applications like heavy-duty vehicles, where using only batteries for energy storage would significantly increase the vehicle's weight, negatively affecting performance, efficiency, and range. In contrast, increasing the fuel cell stack size or hydrogen storage capacity results in a comparatively smaller weight impact, making it a more practical solution [4]. This advantage stems from the fact that hydrogen, which is the most commonly used fuel in FC applications, possesses the highest gravimetric energy density among available energy carriers. This means that hydrogen provides the largest amount of energy per unit of mass, offering significant benefits in energy storage and vehicle weight optimization [5].

For the large-scale deployment of FCEVs, the development of FC technology is one of the key building blocks. The FC technology that has emerged in recent years for vehicle application is the Proton Exchange Membrane (PEM) [6]. This has some key advantages for mobile applications compared to other technologies, such as alkaline and solid oxide. Among other advantages, it operates at low temperatures and does not use toxic elements, thus allowing greater simplicity of the system, it can conduct high current densities, allowing higher power for the same volume or being more compact for the same power, and finally, it has an almost constant efficiency trend over the entire load curve [7]. However, the development of this technology is held back mainly by its costs, which are higher n those of BEVs [8]. This is mainly due to the materials d to make the PEM cell (rare metals for the electrodes and cial polymers for the electrolytic membrane). In addition, the life hours of a cell stack, although they have increased considerably compared to previous years, are still lower than those of an endothermic engine or a BEV drive system [9]. One possibility to reduce costs is to extend the lifetime of the FC [10], [11]. One factor impacting the lifetime of PEM FCs is the current ripple generated by the power converters used to condition their electrical quantities. Several studies have experimentally demonstrated the effect of ripple on the lifetime of the PEM cell, whether it is used as a FC or as an electrolyser [12]–[14].

Indeed, these works have stressed the accelerated aging of fuel cells and electrolyzers under current ripple constraints by using characterization tools such as polarization curves and electrochemical impedance spectroscopy. Important factors in this ageing are the frequency and amplitude of the ripple. Low frequencies are more harmful than high frequencies, while amplitude is always harmful [15]. However, in addition to ageing, it appears that ripple also causes a reduction in cell efficiency [12], [16]–[18]. Over the last few years, two relevant review works have been published in the literature regarding DC/DC converters for FC applications [19], [20]. Both reviews have pointed out the benefits of using interleaved boost converters (classic interleaved, floating interleaved, multidevice interleaved topologies). Indeed, the most important characteristics sought are: high voltage ratio, good weight/volume ratio, efficiency, reliability (in case of power switch failures), and a low current ripple guaranteeing optimized performance of the FC. In this work, it has been chosen to investigate a

Manuscript received xxx, 2024; revised xxx, xxxx. *(Corresponding author: Mattia Ricco)*

P. Pilati, R. Mandrioli, V. Cirimele, and M. Ricco are with the Dept. of Electrical, Electronic and Information Engineering, University of Bologna, Viale del Risorgimento 2, 40126, Bologna, Italy (e-mail: paolo.pilati3@unibo.it; r.mandrioli@unibo.it; vincenzo.cirimele@unibo.it; mattia.ricco@unibo.it).

D. Guilbert is with the GREAH, University of Le Havre Normandie, 75 rue Bellot, 76600, Le Havre, France (e-mail: damien.guilbert@univ-lehavre.fr).

The present work is funded by PNRR M4C2 – Investment 1.4 – Project Mobility "Sustainable Mobility Center" – Code CN00000023 - CUP: J33C22001120001.

synchronous stacked interleaved boost converter (SSIB). On one hand, this topology has been investigated in buck version (especially for electrolyzer applications) [21]–[24]. On the other hand, the boost version has not been considered yet for FC applications. Despite this topology allows reducing input current ripple due to its architecture and operation, the cancellation of input current ripple remains a major concern for FCEVs development. Indeed, the cancellation of input current ripple shall allow optimizing the FC lifetime, avoiding consequently its premature replacement in FCEVs. Therefore, this work proposes a modulation technique of the SSIB to ensure always a ripple-free current on the FC while operating it with the least amount of components possible. This is done through phase shedding to maximise the converter's efficiency and activation or deactivation of a part of the SSIB architecture. The SSIB topology will be discussed in more detail in the following sections.

The article is organized as follows: Section II reports an analysis of the known ripple cancellation technique, Section III explains the proposed modulation technique, Section IV presents numerical validation, and Section V presents experimental analysis.

II. Ripple Cancellation Techniques

As discussed earlier, the current ripple causes accelerated aging of fuel cells. There are several papers in the literature presenting topologies or control techniques that aim to reduce current ripple. A fairly detailed review is done in [25] concerning precisely FC applications. In most cases, however, what is achieved is only a reduction of the ripple or total cancellation at certain precise points of operation. There are topologies capable of eliminating ripple for any point of operation [26]–[28], if specific construction parameters are met, but they are not modular and have low efficiencies. Thus, the decision to consider the SSIB topology is because it is a modular topology able to guarantee the total cancellation of current ripple for any operating point. This modularity also allows for the implementation of efficiency-enhancing techniques, such as phase shedding. A diagram of this topology is shown in Fig. 1. As can be seen, it is a synchronous interleaved boost (SIB) with an additional leg (highlighted in red). The additional leg, called cancellation leg, differs from the others in the presence of a capacitor in series with the inductor, and its detailed operation will be discussed in the following. Considering an N-leg SIB converter, the phase of each leg current is evenly shifted by an electric angle equal to $360°/N$. In this way, the current is shared between all operating legs. Equation (1) expresses the peak-to-peak ripple pattern of the input current $\Delta i_{\mathrm{in,pp}}$ for a boost converter for any operating condition [29]:

$$\Delta i_{\mathrm{in,pp}} = \frac{V_{\mathrm{in}}}{L f_{\mathrm{sw}}} \frac{N}{1-D} \left(\frac{p}{N} - D\right)\left(D - \frac{p-1}{N}\right) \ , \qquad (1)$$

where V_{in} is the input voltage, f_{sw} is the switching frequency, L is the inductance on each leg of the converter, D is the duty cycle and p is a natural index ranging from 0 to N, computed as:

$$p = \mathrm{ceil}(ND) \ . \qquad (2)$$

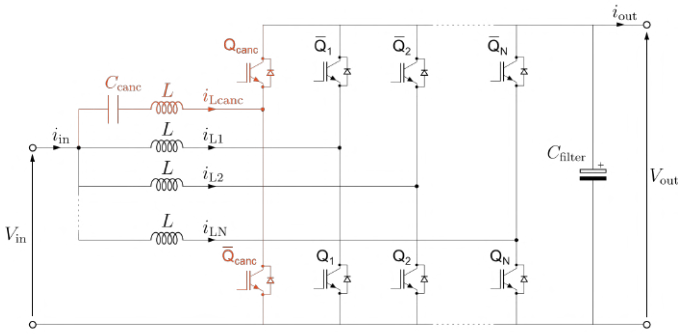

Fig. 1. Generic circuit diagram of a stacked interleaved synchronous boost converter with N legs. The cancellation leg is highlighted in red.

There are therefore N points at which $\Delta i_{\mathrm{in,pp}}$ is zero. In other words, a SIB has N ripple-free working points.

A. Ripple-free via modulation technique

Thus, to cancel the ripple, one could then operate the SIB converter in such a way that it only operates at those points where the ripple is zero. In this way, the minimum and strictly necessary number of components is used, as the cancellation leg is not required. This technique has already been discussed in [30] in the case of an interleaved buck converter. This involves operating the converter at constant duty cycles. The duty cycle in this case is computed as:

$$D = \frac{\mathrm{floor}\left(N\left(1 - \frac{V_{\mathrm{in}}}{V_{\mathrm{out,max}}}\right)\right)}{N} \ , \qquad (3)$$

where $V_{\mathrm{out,max}}$ is the chosen maximum output voltage. However, any variation in the input voltage would result in a corresponding variation in the output voltage. So considering the case of a powertrain powered by a FC, whose voltage varies according to the current supplied, this makes it impossible to work with a constant output voltage. Furthermore, the number of possible duty cycles is finite and directly proportional to the number of legs N. Therefore, to achieve greater flexibility and have more ripple-free duty cycles, it would be necessary to increase the number of legs [31].

B. Ripple-free via cancellation leg

If the converter's output voltage is to be kept constant when the input voltage varies, and it is therefore not possible to operate at a constant duty cycle, the cancellation leg can be used.

The converter is operated such that Q_{canc} conducts when one of the switches Q_{i} ($i = 1, ..., N$) is in conduction, similarly for $\overline{Q}_{\mathrm{i}}$ and $\overline{Q}_{\mathrm{canc}}$. In this way, the cancellation leg presents a behavior opposite to the single-leg Thevenin equivalent circuit of the power legs. The capacitor in series with the inductor blocks the DC component of the current, allowing only the AC component to pass through. Considering the SSIB Thevenin equivalent circuit reported in Fig. 2, the output voltage of the equivalent power leg is represented by v_{p}, while the output voltage of the cancellation leg is represented by v_{c}.

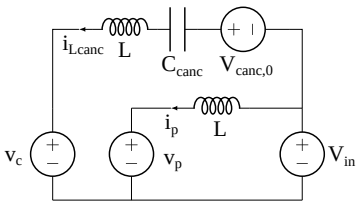

Fig. 2. Thevenin equivalent circuit of an SSIB.

The equivalent power leg switches at a frequency $f_{\mathrm{N}} = N f_{\mathrm{sw}}$ and has an equivalent duty cycle equal to:

$$D_{\mathrm{N}} = \frac{N^2}{1-D}\left(\frac{p}{N} - D\right)\left(D - \frac{p-1}{N}\right) \ . \tag{4}$$

Considering the Thevenin equivalent circuit and using Kirchhoff's voltage law, the following relationship holds:

$$V_{\mathrm{in}} + V_{\mathrm{canc},0} - L\frac{di_{\mathrm{Lcanc}}}{dt} - v_{\mathrm{c}} = 0 \ , \tag{5}$$

$$V_{\mathrm{in}} - L\frac{di_{\mathrm{p}}}{dt} - v_{\mathrm{p}} = 0 \ , \tag{6}$$

where $V_{\mathrm{canc},0}$ is the voltage of the capacitor C_{canc} and i_{p} is the current flowing through the equivalent power leg. Considering a time interval $D_{\mathrm{N}}/f_{\mathrm{N}}$, the main voltages are: $v_{\mathrm{c}} = V_{\mathrm{in}}/(1-D_{\mathrm{N}})$, $v_{\mathrm{p}} = 0$ e $V_{\mathrm{in}} + V_{\mathrm{canc},0} = V_{\mathrm{out}} D_{\mathrm{N}}$. Since, in the considered time interval, the voltage on inductors is constant, the current i_{Lcanc} and i_{p} vary linearly. Thus the derivative di/dt can be written as $\Delta i/\Delta T$, where ΔT in this case is $D_{\mathrm{N}}/f_{\mathrm{N}}$. Therefore, residual ripple Δi_{p} and cancellation leg ripple $\Delta i_{\mathrm{Lcanc}}$ can be obtained as:

$$\Delta i_{\mathrm{p}} = \frac{V_{\mathrm{in}}}{L f_{\mathrm{N}}} D_{\mathrm{N}} \ , \tag{7}$$

$$\Delta i_{\mathrm{Lcanc}} = -\frac{V_{\mathrm{in}}}{L f_{\mathrm{N}}} D_{\mathrm{N}} \ . \tag{8}$$

Thus, the sum of the current in the cancellation leg and the current in the other legs leads to a complete ripple cancellation of the input current; in fact, $\Delta i_{\mathrm{p}} + \Delta i_{\mathrm{Lcanc}} = 0$. With this topology, the current ripple is zero for any load condition. A complete and generalised treatment of this topology has been made in [22], but considering operation as a buck.

From the previous discussion, the cancellation leg differs from the others because it must switch N times faster than the others and must not conduct high currents, but only the ripple. This makes it possible to use different components than the other legs. For example, is possible to use IGBTs for the power legs and Si/SiC MOSFETs for the cancellation leg. In a similar fashion, it might be possible the hybrid utilization of SiC MOSFETs and GaN HEMTs. These could lead also to saving costs. In this case, there would be N legs for power transmission plus an auxiliary leg dedicated solely to ripple cancellation, for a total of $N+1$ legs. A disadvantage of this topology is that it requires more components than the SIB. In addition, it must be taken into consideration that the capacitor used in the cancellation leg must under no circumstances be polarised, as the voltage on that leg is alternating. The use of a polarised capacitor would lead to component failure.

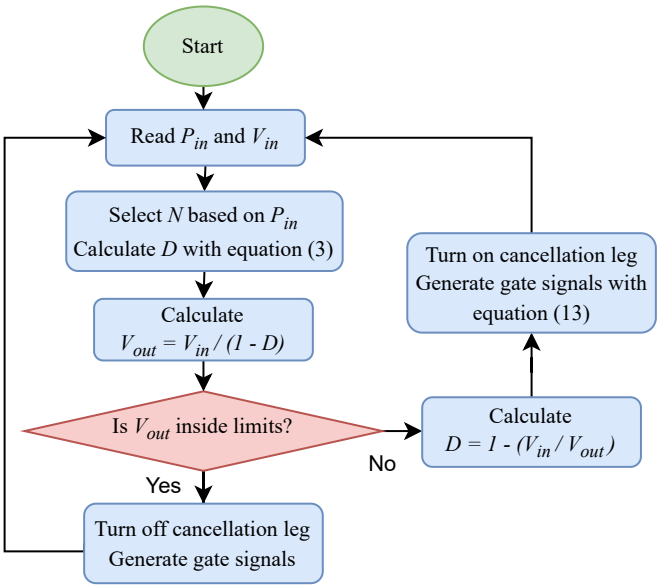

Fig. 3. Generic block diagram of the proposed logic.

III. Proposed Strategy

The proposal of this work is to negotiate the merits of both the cancellation leg and modulation ripple-free. The topology considered is the SSIB, but the number and type of legs used change depending on the load demand and thus the power delivered by the FC P_{in}. It is assumed that the DC bus voltage V_{out} may vary within a certain limit imposed as a design parameter. The converter normally operates as an interleaved boost, with the cancellation leg turned off. The FC's power and voltage in the required operating point are read. Based on this, the number of converter legs is chosen, and phase shedding is performed to improve efficiency. Knowing N and V_{in}, it is possible to calculate the duty to implement the ripple-free control with (3). Having obtained D, it is checked that for the given input voltage, the output voltage is within the imposed limits with the conventional boost input-output relation. If this condition does not occur, the cancellation leg is activated. In this case, the duty must be recalculated so that for the given input voltage, the output voltage respects the set limits. This is done to reduce the number of components conducting each cycle while maintaining the primary demand of having a ripple-free current at the input. A schematic of the described logic is shown in Fig. 3.

A. Leg number regulation and transient handling

Electric transients are caused by a sudden variation in the number of active legs, the carrier phase-shift angle, or the C_{canc} voltage step. When one of these events occurs, both power branches and the cancellation leg experience an erroneous duty cycle value (although only for a short period), which may trigger second-order underdamped oscillation and lead to dangerous current values.

To solve this issue, whenever there is a variation in the number of active legs (either leg addition or removal), all the switches are shut down, allowing for inductor currents to reset to zero. Immediately after, the right amount of legs is sequentially turned on to establish the new current distribution

and carrier phase shift according to the new number of active legs virtually without second-order transients. Clearly, in the short period where the converter is shut down, drive train power delivery is completely entrusted to the energy stored in the DC-link capacitor, as well as to the other power converters typically connected to the high-voltage side. This does not represent an issue because fuel-cell-powered systems present anyway an auxiliary energy storage system to support the so-called short circuit unit (SCU). The SCU short-circuits the fuel cell every 10 seconds for about 100 milliseconds, aiding the moistening of the proton exchange membranes of the cells [32]–[34]. The period required for reconfiguring the legs is largely shorter than the SCU one. In fact, the leg number reconfiguration could be timed in such a way as to coincide with SCU action.

The system can therefore face three types of events:

1) **Cancellation capacitor voltage regulation:** To effectively cancel residual ripple, it is necessary that capacitor C_{canc} experiences the voltage $V_{\mathrm{out}}D_{\mathrm{N}} - V_{\mathrm{in}}$. it should be noted that D_{N} depends on N as per (4). During regular operations where no sudden change of voltage is necessary, the voltage is inherently regulated by the cancellation leg. However, whenever the number of legs is modified, the voltage value changes abruptly, and transients are triggered. To avoid such an issue, the voltage should be gradually regulated by acting on the cancellation leg duty cycle while power legs are active. This will ensure that the cancellation capacitor is brought to the correct voltage value before the switch shut down (i.e., event number 2). During this period ripple-free characteristic is lost, but dangerous transients are avoided.
2) **Switch shut down:** To initiate the leg reconfiguration, all the gate signals are zeroed, thereby enabling the turn-off of the switches. In the immediately following instants, inductor currents begin decreasing (flowing into the switches' antiparallel diodes) until they reach a zero value. In the worst-case scenario (namely, inductor current at its upper peak), the system requires a resetting time of about:
$$t_{\mathrm{res}} = \frac{L}{V_{\mathrm{out}} - V_{\mathrm{in}}}\left(I_{\mathrm{Lx}} + \frac{V_{\mathrm{in}}D}{2f_{\mathrm{sw}}L}\right) , \qquad (9)$$
where I_{Lx} is the average current of the x-th leg. Note that when both cancellation leg switches are turned off, C_{canc} voltage remains constant to the value set during event 1.
3) **Switch sequential turn on:** To reestablish regular current flow into the new leg configuration, every leg bottom switch is turned on sequentially with a time delay of T_{sw}/N (notice that this coincides with the interleaving phase shift). Switches remain in this configuration for the amount of time $I_{\mathrm{Lx}}L/V_{\mathrm{in}}$ necessary to reach the steady-state average current. Once this time has elapsed, regular PWM switching is started. The cancellation leg is activated once the last active leg reaches its steady state value. In the worst-case scenario, the ripple-free operation is restored in about $I_{\mathrm{Lx}}L/V_{\mathrm{in}} + (N-1)/(f_{\mathrm{sw}}N)$.

In essence, the transition from $N = N'$ to $N = N''$ can be achieved by implementing the following procedure. Firstly, the voltage of the cancellation capacitor is regulated to the value $V_{\mathrm{canc},0}(N'')$ (event 1). Secondly, the N' active legs, as well as the cancellation leg, are shut down (event 2). Finally, the new N'' legs are sequentially turned on (event 3).

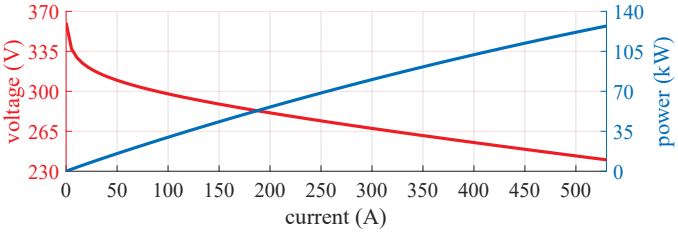

Fig. 4. Polarization curve (in red) and power curve (in blue) of the considered FC.

IV. Numerical Validation

In this section, a numerical example is provided to test the functioning of the proposed architecture and its control strategy. The case study considered concerns a FC designed for heavy-duty vehicles. Its polarization curve and the power characteristic considered are shown in Fig. 4. The polarization curve of a FC consists of its static current-voltage characteristic. Its shape includes three main non-idealities: activation, ohmic and concentration losses [7]. The activation region occurs at low current, while the ohmic region (or linear region) is where the FC is usually operated. The region of concentration losses occurs for currents exceeding the maximum of the FC, so it is not reported in Fig. 4. In general, it is an unwanted operation region since it damages the FC.

The range of variation of the DC bus voltage is considered $750 - 800$ V, so approximately 775 V $\pm\, 3\%$. In this way, if a nominal 400 V battery pack is present in the overall powertrain architecture its DC/DC can operate either as a buck or a boost according to the power flow. The 800 V limit, on the other hand, would allow 1200 V switches to be operated at a utilization factor of 60-70%, thus guaranteeing a certain safety margin. The limits chosen are conservative, as in the case of a nominal 800 V battery directly connected to the DC bus, the voltage variation range could be considered wider.

Two possible strategies are considered to improve the converter's efficiency: phase shedding and phase shedding combined with boundary condition mode (BCM). Having considered an interleaved converter, the first strategy consists of operating a different number of legs according to the required power while keeping the unnecessary ones switched off [35]. This involves operating the converter at a constant frequency f_{sw}. While with the second strategy, the switches are operated in such a way as to obtain soft-switching and thus minimize the switching losses. In this case, soft-switching is achieved without the use of external snubbers but only through the modulation technique. More precisely, the f_{sw} is varied to obtain the minimum peak of the leg current around 0. For a generic SIB, the switching frequency to achieve this condition can be computed as:
$$f_{\mathrm{sw}} = \frac{NV_{\mathrm{in}}D}{2i_{\mathrm{in}}L} . \qquad (10)$$

A converter with 12 power legs is considered. In this way it is possible to operate the system even considering a power

TABLE I
EFFICIENCY CALCULATION PARAMETERS

Parameter	Value	Unit
Leg inductance, L	4	mH
Inductor resistance, R_{L}	35	$m\Omega$
Ferrite mass, m_{Fe}	1	kg
Steinmetz mass coefficient, k	$1.983 \cdot 10^{-3}$	
Steinmetz frequency coefficient, m	1.36	
Steinmetz magnetic coefficient, n	2.86	
Switch resistance, R_{sw}	75	$m\Omega$
Diode resistance, R_{d}	66	$m\Omega$
Diode forward voltage, V_{d}	1.5	V
Turn on losses, E_{on}	$617 \cdot 10^{-6}$	J
Turn off losses, E_{off}	$188 \cdot 10^{-6}$	J
Auxiliaries losses, P_{aux}	10	W

derating in the event of a single or multiple leg failure. This also allows currents of up to around 45 A on each leg of the converter, thus enabling the use of smaller components. For simplicity only one switch model is used in the efficiency calculation: the STMicroelectronics SCTH60N120G2-7 MOSFET. For the first strategy, the switching frequency f_{sw} is set to 10 kHz. Conversely, the second strategy presents variable frequency from 1 to 10 kHz. The upper limit, in this case, is chosen to have a worst-case switching frequency of the cancellation leg below 150 kHz, which is a standard limit in regulation on electromagnetic compatibility [36].

For efficiency calculation, losses in capacitors are not considered, but only those in inductors, switches, diodes, and auxiliaries. Losses in the inductors are divided into core and conduction losses. The core losses P_{Fe} are computed based on the Steinmetz equation (see, [37]) considering a ferrite core:

$$P_{\mathrm{Fe}} = m_{\mathrm{Fe}} k f_{\mathrm{sw}}^{m} \hat{B}^{n} \ , \tag{11}$$

in which $\hat{B}$ is the peak magnetic flux density in the inductor core, m_{Fe} is the ferromagnetic core weight, k, m, and n are coefficients that depend on the type of material used to make the ferromagnetic core. The switch losses are divided into conduction and switching losses. Conduction losses are evaluated by referring to MOSFET R_{sw}. While commutation losses are computed based on the switching energy listed on the datasheet. Power losses considered for diodes include reverse recovery losses. The power absorbed by the auxiliaries for each switch is assumed to be constant. All the useful values used for the efficiency calculation are listed in Table I.

The case of SIB was also considered for comparison. The results of the analytical calculation are shown in Fig. 5. Fig. 6 gives a direct comparison of the three cases. As can be seen, the SIB always has a higher efficiency as it has fewer components. Considering instead only the case of the SSIB, it can be seen that the BCM achieves only a slight improvement in efficiency at partial loads, but for loads above 60% of maximum power, efficiency drops rapidly. This is due to the low switching frequency, which increases the rms value of the leg currents. To enable a comparison, the 4-point efficiency $\eta_{4\mathrm{point}}$ is considered. It is computed as:

$$\eta_{4\mathrm{point}} = \frac{1}{4}(\eta_{25\%} + \eta_{50\%} + \eta_{75\%} + \eta_{100\%}) \ . \tag{12}$$

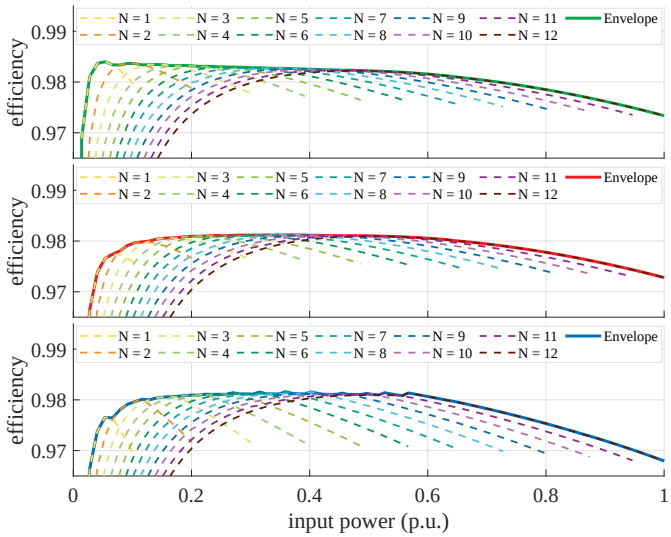

Fig. 5. Efficiency curves varying the number of legs from $N = 1$ to $N = 12$ and their upper envelope, considering on top the SIB, in the middle the SSIB, and at the bottom the SSIB with BCM.

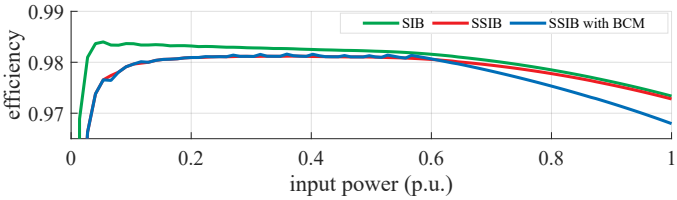

Fig. 6. Comparison between phase shedding and phase shedding with BCM.

where $\eta_{25\%}$, $\eta_{50\%}$, $\eta_{75\%}$, and $\eta_{100\%}$ are the efficiency value at 25%, 50%, 75%, and 100% of the load, respectively. The results of the three considered cases are 97.9%, 97.8%, and 97.6% for the SIB, SSIB, and the SSIB with BCM, respectively. In light of these results, it can be seen how convenient it is to deactivate the cancellation leg if ripple elimination is already achieved through the duty cycle. Furthermore, given the marginal impact of the BCM on efficiency, it is decided not to be considered in the following discussion.

Before the experimental tests, the phase shedding logic of the SSIB is simulated using PLECS, focusing solely on the fuel cell and its converter. The load is modeled as a controlled current source, with a ramp-shaped power demand applied to the fuel cell, mimicking a request from the vehicle's energy management system.

Fundamental to the proper functioning of the SSIB is carrier synchronism, as the switching frequency of the cancellation leg depends on the number of power legs used N. Using different carriers for the cancellation leg and the power legs leads to a loss of synchronism when inserting new legs. Because the number of active power legs changes, the carrier frequency of the cancellation leg changes. This can then lead to an unwanted phase shift relative to the other carriers, thus losing the ability to cancel ripple. To overcome this problem, the gate signal of the cancellation leg $s_{\mathrm{canc}}(t)$ has been generated as:

$$s_{\mathrm{canc}}(t) = \sum_{\mathrm{i}=1}^{N} s_{\mathrm{i}}(t) - \mathrm{floor}(ND) - N_{\mathrm{off}} \ , \tag{13}$$

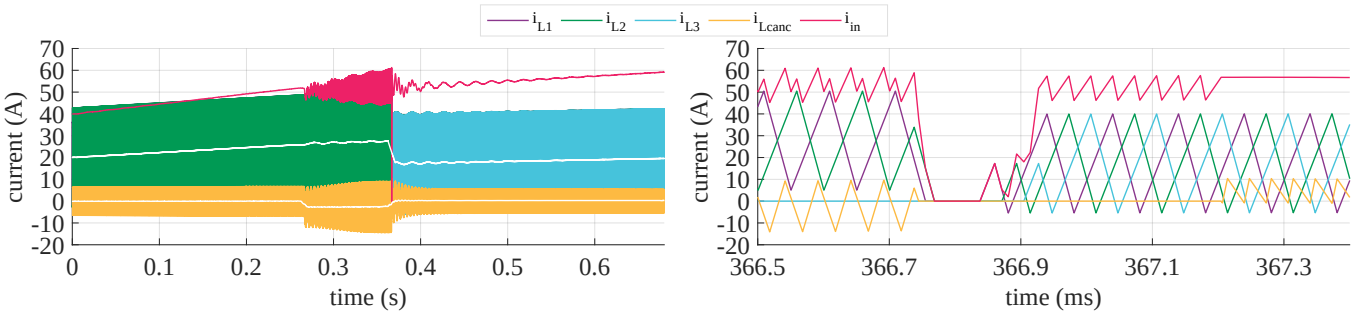

Fig. 7. Power legs, cancellation, and input currents under active leg number rearrangement from $N' = 2$ to $N'' = 3$. The right frame shows a detailed view of the currents during the leg transition. White lines on the left frame are the moving average of power legs and cancellation currents.

where $s_{\mathrm{i}}(t)$ are the various gate signals of the power legs and N_{off} are the unused converter legs.

To validate the outcomes related to ripple-free, phase-shedding, and transient handling, a time domain plot of the power legs, cancellation, and input currents is displayed in Fig. 7, considering an active leg number rearrangement from $N' = 2$ to $N'' = 3$. As visible in the left frame, the FC current i_{in} is under ripple-free condition thanks to the action of the cancellation leg (see current i_{Lcanc}). At the time instant 268 ms, the voltage of the cancellation capacitor C_{canc} is gradually regulated in view of the leg number increment (see event 1 in Subsection III-A). During this event, and as anticipated, the current i_{in} loses its ripple-free characteristic. Additionally, the cancellation current i_{Lcanc} experiences a non-zero moving average, meaning that energy is being transferred from/to the cancellation capacitor. Once the voltage regulation is concluded (see instant 366.7 ms), the system experiences events 2 and 3 in rapid sequence. In fact, by looking at the detailed view of the right frame, all the currents shut down in about 50 μs. After about 70 μs, legs are sequentially turned on, and the expected steady state current is established in less than 100 μs without any appreciable transient. At the instant 367.2 ms, the cancellation leg is again enabled and the i_{in} experiences again a ripple-free condition. It is important to notice that the system remains in a shut-down state for less than 1 ms. Such time is sharply shorter than the times typically experienced during SCU action [34]. Clearly, the same sequence of events can be replicated for any number N' and N''.

V. Experimental Validation

In order to test the impact of the cancellation leg on current ripple and its effectiveness if the converter already operates at a ripple-free duty cycle, a series of experimental tests are carried out. In this case, the converter is realised with seven power legs and one cancellation leg. The topology considered and discussed above is tested in the laboratory at inverted power flow, i.e. as if operating as a buck.

The laboratory setup is divided into two: the main part, with the converter under test, and the acquisition and control part. A photo of the setup is reported in Fig. 8. The main part consists of a TDK-Lambda GEN 750W/1500W series power supply, two capacitors placed in parallel to act as the DC bus, four PCBs in parallel with the actual converter (each PCB consists of an IGBT-based H bridge and its circuits to generate the gate signals), the inductors of the various legs, two capacitors in series to make the

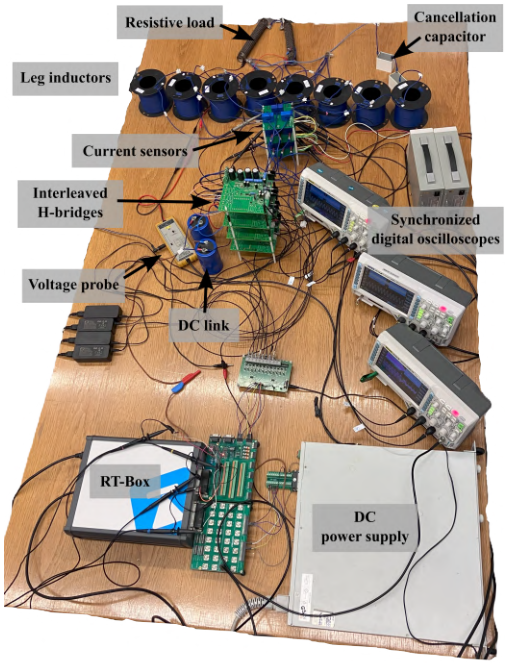

Fig. 8. View of the whole experimental setup.

TABLE II
Experimental System Parameters

Parameter	Components Count	Value	Unit
DC link capacitance, C_{DC}	2	1	mF
Leg inductance,L_{i}	8	1.73	mH
Leg resistance,R_{i}	8	0.73	Ω
Cancellation capacitance, C_{canc}	2	100	μF
Load resistor, R_{load}	2	10	Ω
Input voltage, V_{in}	ND	70	V
Switching frequency, f_{sw}	ND	1	kHz

capacitance of the cancellation leg and two resistors in series for the load. The values of the various components and the various quantities used are collected in Table II. The acquisition and control part consists of three RIGOL DS1054Z oscilloscopes to acquire and display current and voltage waveforms, eight LEM LA 55-P current sensors, a Pico Technology TA041 voltage probe, the RT-Box-1 to control the converter, and a PC.

In order to achieve phase shedding, it is necessary to control the gate signals of the individual switches, otherwise the individual leg will never shed. In this case, the dynamic phase shedding is not possible so tests are therefore carried out in the 7−, 5−, and 3−leg cases. For each of these configurations,

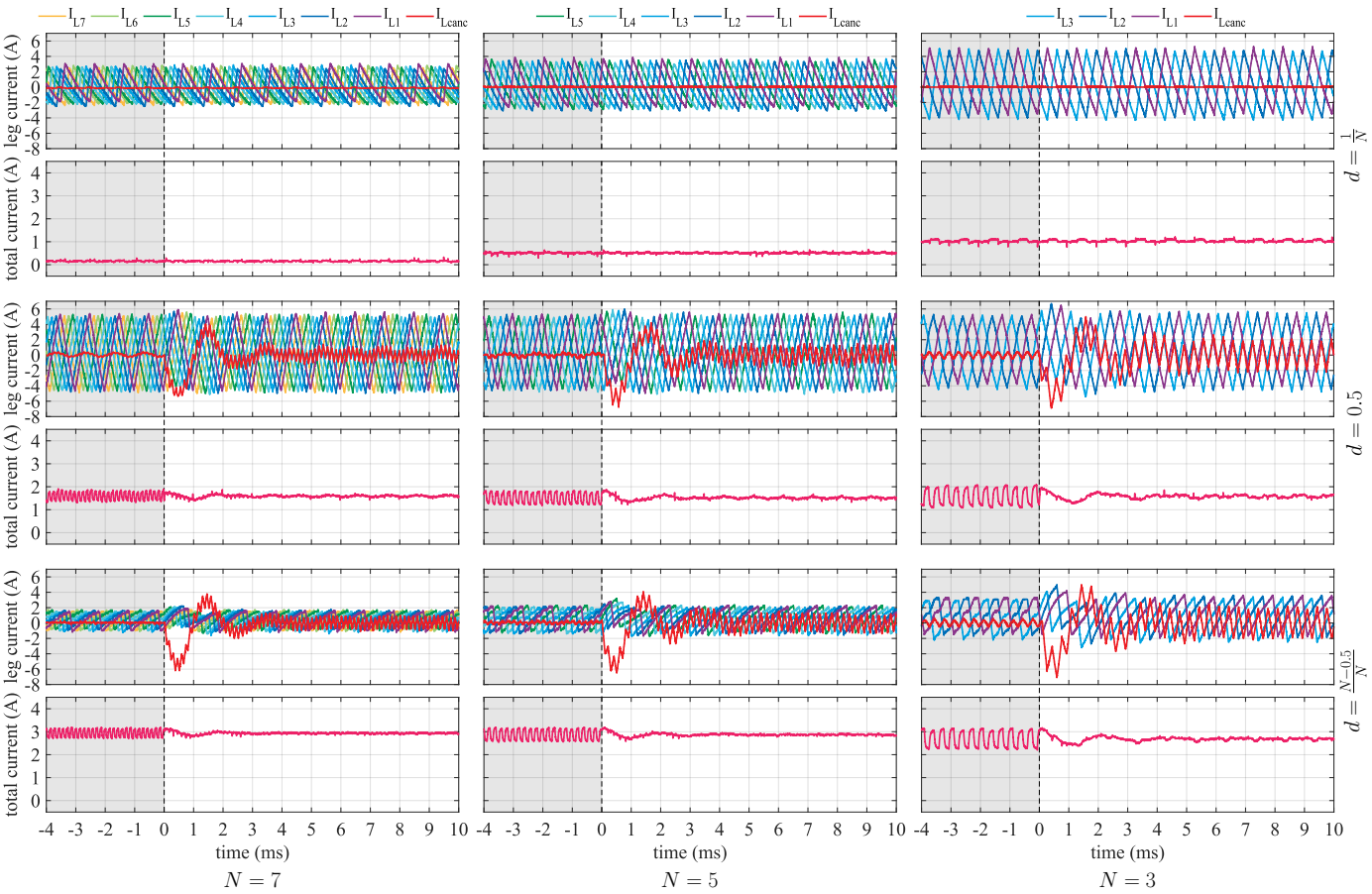

Fig. 9. Experimental results obtained for the leg and load currents: on the left are the cases with $N = 7$, in the center those with $N = 5$, and on the right those with $N = 3$, while at the top are the cases with $d = 1/N$, in the middle those $d = 1/2$, and at the bottom those with $d = (N - 0.5)/N$. The grey area represents the time before the activation of the cancellation leg.

a series of three duty cycles common to all are used, namely $D = 1/N$, $D = 1/2$, and $D = (N - 0.5)/N$. In this way, the first is a ripple-free point for all of them, the second is a point common to all where ripple is present, and the third is the case with the largest ripple amplitude for all three.

The generation of the carrier and modulation signals is performed in the PLECS environment. The various gate signals are then generated by the RT-Box which sends them as a digital signal to the corresponding board. To stress the effect of the cancellation leg the maximum switching frequency used for the power legs is 1 kHz. In this way, with the same inductors, a higher current ripple is obtained.

In each test, the action of the converter is tested with and without the cancellation leg. Data acquisition is synchronized with the activation of the cancellation leg. The experimental results are shown in Fig. 9 where are reported the different leg currents and the total current. The instant when the cancellation leg is switched on is chosen as the time axis reference: the gray area indicates when it is switched off.

As can be seen, in all tests with $D = 1/N$ the effect of the cancellation leg is minimal or negligible, as the converter already operates at a point where no ripple is present. So in this case it is not necessary to use it or keep it switched on. In the remaining cases, switching on the cancellation leg always leads to an improvement of the output current, cancelling the ripple. This is particularly noticeable in the case with $N = 3$, where the reduced number of legs naturally leads to a higher ripple.

Another phenomenon that can be appreciated from the acquisitions made is the insertion transient of the cancellation leg, which for short periods can lead to current values even higher than those circulating in the other legs. The transient, however, dies out very quickly, as its duration is of the order of a few ms. This raises an issue in the case that this type of converter is operated in an open loop, about the sizing of the switches of the cancellation leg: it could be sized using smaller switches than the power legs, since under normal conditions, if it is always active and the number of legs does not change, the current flowing through it would only consist of ripple. But, in a dynamic case in which the insertion and deactivation of the leg can occur more frequently, it is advisable to size the switches considering also the overload of the component. Because the number and the amplitude of these transients can lead to premature ageing of the converter, so it is an aspect to be considered during design. However, these considerations only apply in the case where the converter is operated in an open loop. In the more realistic case of closed-loop control, the amplitude of the current transients can be contained, allowing smaller switches to be used for the cancellation leg. It can also be seen how the switching frequency of the cancellation leg varies with the number of power legs used.

Finally, a converter efficiency assessment is carried out to validate the results of the analytical efficiency analysis. To

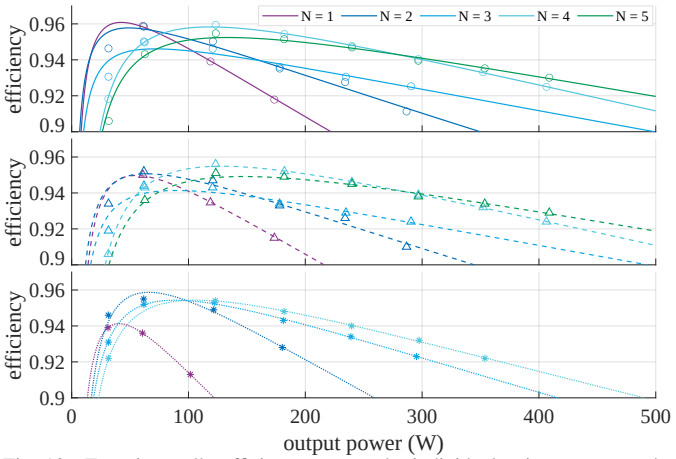

Fig. 10. Experimentally efficiency curves, the individual points represent the measurement made while the lines represent their interpolation according to [35]: on top the SIB, in the middle the SSIB, and at the bottom the SSIB with BCM.

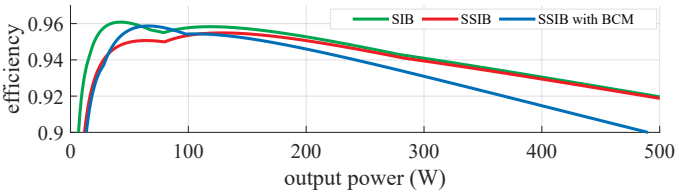

Fig. 11. Comparison between the upper envelope of the experimental efficiency curves.

this end, a ZES Zimmer LMG671 wattmeter is employed. The number of legs considered for the efficiency calculation is limited to 5, and the switching frequency considered is 3 kHz. For the BCM case, the switching frequency is varied between 1 and 10 kHz. In the latter case in particular, the number of legs is limited to 4 due to limitations on the maximum frequency of the cancellation leg switches. For every previously considered scenario (SIB, SSIB, and SSIB with BCM), the efficiency is measured, and then the results are interpolated according to [35].

The results for every considered case are reported in Fig. 10, while their comparison is shown in Fig. 11. The obtained trends are consistent with the results obtained in the analytical analysis, confirming that the cancellation leg should be activated only when needed. The major difference pertains to the BCM trend, which exhibits a higher level of efficiency in comparison to the SIB for power outputs below 100 W. Such a phenomenon is related to the use of a low-scale prototype. Benefits related to phase shedding are evident. Indeed, for high values of power, a higher leg number presents the best performance. On the other hand, at low power, it is necessary to turn off most of the legs to ensure optimal efficiency. The experimental 4-point efficiencies are 93.9%, 93.7%, and 92.7% for the SIB, SSIB, and the SSIB with BCM, respectively. Such a result is in agreement with what was anticipated in section IV.

VI. Conclusions

This work focuses on mitigating the current ripple in fuel cells with the aim of increasing their lifetime. To cancel the ripple, two possibilities are considered: either via a modulation technique to operate the converter in ripple-free condition or by using a stacked interleaved boost type converter. The second choice is selected because simply disabling the additional cancellation leg would fall into the interleaved boost. As a control for the converter, it is proposed to operate it always at ripple-free duty cycle and only use the cancellation leg when it is not possible to remain within the limits imposed on the output voltage. An efficiency analysis is carried out, and phase shedding has proven to be a valid option to increase the converter's efficiency and thus the entire system at loads less than 40% of the maximum value. Transient handling and the number of leg reconfiguration discussion procedure has been provided. Simulation results show that the ripple can be cancelled out for any load condition, with the exception of transients caused by the insertion or disconnection of new legs, in which case this condition is waived in order to avoid dangerous current peaks.

Finally, experimental tests were carried out to assess the cancellation leg's real impact on the system and to compare the efficiencies with and without the cancellation leg. The results showed that it is not necessary to use the cancellation leg at points where ripple-free is already guaranteed by the duty cycle. In the remaining cases, the cancellation leg always improves the total current, almost eliminating the ripple. Furthermore, the experimental efficiency analysis shows that what was hypothesised is valid, thus making it not recommended to use the cancellation leg when not required.

References

[1] M. Barresi, D. De Simone, L. Piegari, and R. Scalabrin, "Novel current source converter for integrating multiple energy storage systems," *Energies*, vol. 17, no. 11, p. 2495, 2024.

[2] K. Turoń, "Hydrogen-powered vehicles in urban transport systems–current state and development," *Transportation Research Procedia*, vol. 45, pp. 835–841, 2020.

[3] C. Cunanan, M.-K. Tran, Y. Lee, S. Kwok, V. Leung, and M. Fowler, "A review of heavy-duty vehicle powertrain technologies: Diesel engine vehicles, battery electric vehicles, and hydrogen fuel cell electric vehicles," *Clean Technologies*, vol. 3, no. 2, pp. 474–489, 2021.

[4] M. Kandidayeni, J. P. F. Trovão, L. Boulon, and S. Kelouwani, "Health-wise energy management strategies in fuel cell hybrid electric vehicles: Tools to optimize performance and reduce operational costs," *IEEE Electrification Magazine*, vol. 12, no. 2, pp. 80–88, 2024.

[5] N. Rusman and M. Dahari, "A review on the current progress of metal hydrides material for solid-state hydrogen storage applications," *International Journal of Hydrogen Energy*, vol. 41, no. 28, pp. 12 108–12 126, 2016.

[6] M. İnci, M. Büyük, M. H. Demir, and G. İlbey, "A review and research on fuel cell electric vehicles: Topologies, power electronic converters, energy management methods, technical challenges, marketing and future aspects," *Renewable and Sustainable Energy Reviews*, vol. 137, p. 110648, 2021.

[7] G. Kaur, *PEM fuel cells: fundamentals, advanced technologies, and practical application*. Elsevier, 2021.

[8] Y. Manoharan, S. E. Hosseini, B. Butler, H. Alzhahrani, B. T. F. Senior, T. Ashuri, and J. Krohn, "Hydrogen fuel cell vehicles; current status and future prospect," *Applied Sciences*, vol. 9, no. 11, p. 2296, 2019.

[9] M. M. Tellez-Cruz, J. Escorihuela, O. Solorza-Feria, and V. Compañ, "Proton exchange membrane fuel cells (pemfcs): Advances and challenges," *Polymers*, vol. 13, no. 18, p. 3064, 2021.

[10] J. Wu, X. Z. Yuan, J. J. Martin, H. Wang, J. Zhang, J. Shen, S. Wu, and W. Merida, "A review of pem fuel cell durability: Degradation mechanisms and mitigation strategies," *Journal of Power Sources*, vol. 184, no. 1, pp. 104–119, 2008.

[11] J. Zhang, Q. Xun, M. Liserre, and H. Yang, "Health-aware bi-level optimization of component sizing and real-time energy management in fuel cell hybrid electric trucks," *IEEE Transactions on Industry Applications*, 2024.

[12] J. E. Valdez-Resendiz, J. C. Rosas-Caro, V. M. Sanchez, and A. R. Lopez-Nuñez, "Experimental study of a fuel cell stack performance operating with a power electronics converter with high-frequency current ripple," *International Journal of Hydrogen Energy*, 2024.

[13] E. Pahon, M.-C. Péra, D. Bouquain, and D. Hissel, "Impact of current ripples on the durability of proton exchange membrane fuel cells based on two ageing datasets," *Data in Brief*, vol. 45, p. 108601, 2022.

[14] F. Parache, H. Schneider, C. Turpin, N. Richet, O. Debellemanière, É. Bru, A. T. Thieu, C. Bertail, and C. Marot, "Impact of power converter current ripple on the degradation of pem electrolyzer performances," *Membranes*, vol. 12, no. 2, p. 109, 2022.

[15] Y. Zhan, Y. Guo, J. Zhu, B. Liang, and B. Yang, "Comprehensive influences measurement and analysis of power converter low frequency current ripple on pem fuel cell," *International Journal of Hydrogen Energy*, vol. 44, no. 59, pp. 31 352–31 359, 2019.

[16] H. P. Buitendach, R. Gouws, C. A. Martinson, C. Minnaar, and D. Bessarabov, "Effect of a ripple current on the efficiency of a pem electrolyser," *Results in Engineering*, vol. 10, p. 100216, 2021.

[17] B. Wahdame, L. Girardot, D. Hissel, F. Harel, X. François, D. Candusso, M. C. Pera, and L. Dumercy, "Impact of power converter current ripple on the durability of a fuel cell stack," in *2008 IEEE international symposium on industrial electronics*. IEEE, 2008, pp. 1495–1500.

[18] Y. Zhan, Y. Guo, J. Zhu, and L. Li, "Input current ripple reduction and high efficiency for pem fuel cell power conditioning system," in *2017 20th International Conference on Electrical Machines and Systems (ICEMS)*. IEEE, 2017, pp. 1–6.

[19] A. Kolli, A. Gaillard, A. De Bernardinis, O. Bethoux, D. Hissel, and Z. Khatir, "A review on dc/dc converter architectures for power fuel cell applications," *Energy Conversion and Management*, vol. 105, pp. 716–730, 2015.

[20] H. Wang, A. Gaillard, and D. Hissel, "A review of dc/dc converter-based electrochemical impedance spectroscopy for fuel cell electric vehicles," *Renewable Energy*, vol. 141, pp. 124–138, 2019.

[21] J. Wibben and R. Harjani, "A high-efficiency dc–dc converter using 2 nh integrated inductors," *IEEE Journal of Solid-State Circuits*, vol. 43, no. 4, pp. 844–854, 2008.

[22] M. A. Alharbi, M. S. Dahidah, S. A. Ali, S. A. Ethni, and V. Pickert, "Ripple-free multiphase interleaved stacked converter for high-power applications," *IEEE Transactions on Power Electronics*, vol. 37, no. 12, pp. 14 770–14 780, 2022.

[23] L. Zhang, M. Han, W. Bao, Y. Dong, Y. Fan, and H. Liu, "Low-ri high-efficiency ac-dc rectifier with auxiliary compensator for hydrc production," *IET Power Electronics*, vol. 16, no. 12, pp. 2091–2 2023.

[24] X. Guo, S. Zhang, Z. Liu, L. Sun, Z. Lu, C. Hua, and J. M. Guerrero, "A new multi-mode fault-tolerant operation control strategy of multiphase stacked interleaved buck converter for green hydrogen production," *International Journal of Hydrogen Energy*, vol. 47, no. 71, pp. 30 359–30 370, 2022.

[25] Y. Zhan, Y. Guo, J. Zhu, L. Li, B. Yang, and B. Liang, "A review on mitigation technologies of low frequency current ripple injected into fuel cell and a case study," *International Journal of Hydrogen Energy*, vol. 45, no. 46, pp. 25 167–25 190, 2020.

[26] J. C. Rosas-Caro, F. Mancilla-David, J. C. Mayo-Maldonado, J. M. Gonzalez-Lopez, H. L. Torres-Espinosa, and J. E. Valdez-Resendiz, "A transformer-less high-gain boost converter with input current ripple cancelation at a selectable duty cycle," *IEEE Transactions on Industrial Electronics*, vol. 60, no. 10, pp. 4492–4499, 2012.

[27] M. J. Schutten, R. L. Steigerwald, and J. A. Sabaté, "Ripple current cancellation circuit," in *Eighteenth Annual IEEE Applied Power Electronics Conference and Exposition, 2003. APEC'03.*, vol. 1. IEEE, 2003, pp. 464–470.

[28] J. Wang, W. G. Dunford, and K. Mauch, "Analysis of a ripple-free input-current boost converter with discontinuous conduction characteristics," *IEEE transactions on power electronics*, vol. 12, no. 4, pp. 684–694, 1997.

[29] S. Zhang, "Analysis and minimization of the input current ripple of interleaved boost converter," in *2012 Twenty-Seventh Annual IEEE Applied Power Electronics Conference and Exposition (APEC)*. IEEE, 2012, pp. 852–856.

[30] K. Drobnic, G. Grandi, M. Hammami, R. Mandrioli, M. Ricco, A. Viatkin, and M. Vujacic, "An output ripple-free fast charger for electric vehicles based on grid-tied modular three-phase interleaved converters," *IEEE Transactions on Industry Applications*, vol. 55, no. 6, pp. 6102–6114, 2019.

[31] R. Mandrioli, M. Ricco, M. Hammami, A. Viatkin, and G. Grandi, "A ripple-free output current interleaved dc/dc converter design algorithm for ev charging," in *2021 22nd IEEE international conference on industrial technology (ICIT)*, vol. 1. IEEE, 2021, pp. 292–297.

[32] G. Gupta, B. Wu, S. Mylius, and G. J. Offer, "A systematic study on the use of short circuiting for the improvement of proton exchange membrane fuel cell performance," *International Journal of Hydrogen Energy*, vol. 42, no. 7, pp. 4320–4327, 2017.

[33] F. Grumm, M. Schumann, C. Cosse, M. Plenz, A. Lücken, and D. Schulz, "Short circuit characteristics of pem fuel cells for grid integration applications," *Electronics*, vol. 9, no. 4, 2020.

[34] M. Rimondi, R. Mandrioli, V. Cirimele, L. K. Pittala, M. Ricco, and G. Grandi, "Design of an integrated, six-phase, interleaved, synchronous dc/dc boost converter on a fuel-cell-powered sport catamaran," *Designs*, vol. 6, no. 6, 2022.

[35] J. W. Kolar, F. Krismer, Y. Lobsiger, J. Muhlethaler, T. Nussbaumer, and J. Minibock, "Extreme efficiency power electronics," in *2012 7th International Conference on Integrated Power Electronics Systems (CIPS)*. IEEE, 2012, pp. 1–22.

[36] A. Mariscotti, "Critical review of emc standards for the measurement of radiated electromagnetic emissions from transit line and rolling stock," *Energies*, vol. 14, no. 3, p. 759, 2021.

[37] C. W. T. McLyman, *Transformer and inductor design handbook*. CRC press, 2004.

Paolo Pilati (Student Member, IEEE) received the B.Eng. and M.Sc. degrees in electrical engineering from the Alma Mater Studiorum - University of Bologna, Bologna, Italy, in 2019 and 2022, respectively. He is currently working toward the Ph.D. degree in Photovoltaics within the Department of Electrical, Electronic, and Information Engineering at the University of Bologna, Bologna, Italy.

Riccardo Mandrioli (Senior Member, IEEE) received the Ph.D. degree in Biomedical, Electrical, and System Engineering in 2023 from the University of Bologna, Bologna, Italy.

Currently, he is a Tenure Track Assistant Professor with the Department of Electrical, Electronic, and Information Engineering, University of Bologna. In 2022, he was a Visiting Scientist with the Chair of Power Electronics, Kiel University, Kiel, Germany. His research interests deal with power electronic converter topologies and modulations.

Dr. Mandrioli was the winner of the IEEE IES – Italy Section Chapter 2024 PhD Thesis Award and the MDPI Electronics 2023 Best PhD Thesis Award. He was the recipient of the IEEE IES SYPA Award of the IEEE CPE-POWERENG 2023 and IECON 2025, the IEEE ENERGYCON 2020 Best Paper Award, the IEEE IES SYP Congress 2025 Travel Grant, and the IEEE ICDCM 2025 Best Reviewer Award. He is an Associate Editor for IEEE ACCESS, an Editorial Board Member for the *Electricity*, *Designs*, and *Discover Electronics*, and IEEE Italy Section Entrepreneurship Committee Member.

Vincenzo Cirimele (Senior Member, IEEE) received the M.Sc. (summa cum laude) and Ph.D. degrees in electrical engineering from the Politecnico di Torino, Turin, Italy, in 2013 and 2017, respectively, and the Ph.D. degree in electronics engineering from the Université Paris-Saclay, Gir-sur-Yvette, France, in 2017. Currently, he is an Associate Professor with the Department of Electrical, Electronic, and Information Engineering, Alma Mater Studiorum University of Bologna, Bologna, Italy. From 2020 to 2021, he was a Technical Responsible for the R&D and Innovation Group of the company Movyon s.p.a., Florence, Italy of Autostrade per l'Italia Group where he supervised projects related to energy sustainability and development of highway electric mobility. Since May 2019 he is among the founders of the start-up Enermove s.r.l dealing with wireless charging systems for electric vehicles in the industrial field. From 2017 to 2020, he held the position of an Assistant Professor with the Department of Energy, Politecnico di Torino. His research interests include technologies for electric mobility, inductive power transmission, electromagnetic modeling and simulation, and power electronics. Prof. Cirimele acts as a Deputy Editor for IET Power Electronics and an Associate Editor for the journals IEEE Transactions on Transportation Electrification and Wireless Power Transfer.

Damien Guilbert (Senior Member, IEEE) was born in Paris, France, in 1987. He received the M.Sc. degree in electrical engineering and control systems and the Ph.D. degree in electrical engineering from the University of Technology of Belfort-Montbéliard, Belfort, France, in 2011 and 2014, respectively, and the habilitation à diriger des recherches in electrical engineering from the University of Lorraine, Longwy, France, in 2022. From 2016 to 2023, he was an Associate Professor with the University of Lorraine, France and a permanent member of the Group of Research in Electrical Engineering of Nancy (GREEN) Laboratory. Since 2023, he has been a Full Professor with the University of Le Havre Normandy, Le Havre, France, and has been a permanent member of the Group of Research in electrical engineering and automatic control of le Havre (GREAH). His current research interests include power electronics for electrolyzer applications, electrolyzer modeling and emulation, and energy management of multisource systems relying on renewable energy sources and hydrogen technologies.

Mattia Ricco (Senior Member, IEEE) received the M.Sc. degree (cum laude) in electronic engineering from the University of Salerno, Fisciano, Italy, in 2011, and the Ph.D. double degrees in electrical and electronic engineering and in information engineering from the University of Cergy-Pontoise, Cergy, France, and the University of Salerno, in 2015. From 2015 to 2018, he was a Postdoctoral Research Fellow with the Department of Energy Technology, Aalborg University, Aalborg, Denmark. From 2018 to 2021, he was a Senior Assistant Professor (Tenure Track) and has been an Associate Professor with the Department of Electrical, Electronic, and Information Engineering, University of Bologna, Bologna, Italy, since 2021. His research interests include modular multilevel converters, battery management system, electric vehicle chargers, field-programmable gate array-based controllers, and photovoltaic systems. Prof. Ricco was the recipient of the IEEE ENERGYCON 2020 Best Paper Award. He is an Associate Editor for IEEE Transactions on Industrial Electronics and an Editor for IET Power Electronics.